FUNDAMENTAL DEPENDENCIES IN ANGLE-DELAY-DOPPLER IN WIRELESS CHANNELS

Akbar M. Sayeed

Electrical and Computer Engineering
University of Wisconsin-Madison
akbar@engr.wisc.edu

ABSTRACT

The degrees of freedom in a wireless channel determine its statistics and capacity. The degrees of freedom in turn depend on the number and spatial distribution of physical propagation paths in the environment as well as the signal space dimensions (number of antennas, bandwidth). In this paper, we use a virtual representation of time- and frequency-selective MIMO channels to relate the degrees of freedom to the physical propagation paths. The virtual representation is characterized by virtual channel coefficients in angle-delay-Doppler space. It induces a partitioning of paths that reveals the contribution of each path to the degrees of freedom as well as fundamental dependencies in angle, delay and Doppler that constrain the degrees of freedom. As the signal space dimensions increase, the degrees of freedom increase whereas the statistics of the virtual channel coefficients deviate from Gaussian (Rayleigh) to "specular" in which the amplitude of the coefficients is deterministic and the channel variations are manifested solely in the phase. Implications of the angle-delay-Doppler dependencies on channel structure and capacity are discussed, which are particularly relevant to ultra-wideband systems.

1. INTRODUCTION

The capacity and diversity afforded by a time- and frequency-selective MIMO (TF-MIMO) channel is due to the spatial distribution of propagation paths and the relative motion of the transmitter and receiver arrays. The distribution of propagation paths, in conjunction with signal space dimensions, determine the structure and degrees of freedom (DoF) of a TF-MIMO channel, which in turn determines the channel statistics and capacity. Virtually all existing analyses of MIMO channels are based on the assumption of Rayleigh fading which implicitly assumes an infinite number of paths. In reality, the number of dominant paths is finite.

In this paper, we investigate the statistics and structure of TF-MIMO channels under the assumption of a finite number of paths. Our study is based on a virtual representation of TF-MIMO channels that captures the essence of channel-signal space interaction in time, frequency and space [1, 2]. Each physical scatterer can be associated with a unique Angle of Departure (AoD), Angle of Arrival (AoA), delay, and Doppler shift. The virtual representation replaces the actual physical scatterers with virtual scatterers associated with fixed uniformly spaced AoD's, AoA's, delays and Doppler shifts on a four-dimensional (4D) grid. The grid spacings in the four dimensions correspond to the resolutions in time, frequency and the two spatial dimensions that are determined by the signaling bandwidth, duration, and array apertures, respectively. The virtual representation yields many useful insights. Particularly relevant to this work, it induces a partitioning of paths in angle-delay-Doppler that explicitly reveals the contribution of each path to channel DoF. It also unravels fundamental dependencies in angle-delay-Doppler that constrain the DoF.

The study in this paper yields two important insights. First, in the virtual spatial domain (beamspace), the virtual coefficients exhibit lesser selectivity in time and frequency compared to the actual coefficients.[1] Furthermore, the virtual spatial matrices corresponding to distinct virtual delays exhibit disjoint sets of dominant coefficients, as supported by some preliminary results based on measured data. Second, as the signal space dimensions increase, the assumption of Rayleigh fading gets violated. In essence, the variation in virtual channel coefficients over time is solely governed by phase variations (rather than phase and amplitude variation in Rayleigh fading). We present some preliminary results to show that this deviation from Rayleigh fading does not affect the ergodic capacity but could significantly improve outage capacity performance at moderate to low SNRs (< 10dB). The above implications of angle-delay-Doppler dependencies could be exploited in the design of non-coherent signaling schemes and multiuser receivers for ultra-wideband systems.

2. A PHYSICAL MODEL FOR MIMO CHANNELS

Consider a transmitter array with P elements and a receiver array with Q elements. We want to represent the TF-MIMO channel over a signaling duration T and bandwidth W. In the absence of noise, the transmitted and received signals are related as

$$\boldsymbol{x}(t) = \int_{-W/2}^{W/2} \boldsymbol{H}(t,f)\boldsymbol{S}(f)e^{j2\pi ft}df, \;\; -T/2 \leq t \leq T/2, \quad (1)$$

where $\boldsymbol{s}(t)$ is the P-dimensional transmitted signal, $\boldsymbol{S}(f)$ is the Fourier transform of the transmitted signal, $\boldsymbol{x}(t)$ is the Q-dimensional received signal, and $\boldsymbol{H}(t,f)$ denotes the *time-varying frequency response matrix* coupling the transmitter and receiver elements.

For simplicity we focus on one-dimensional ULAs of antennas with antenna spacing d. The channel matrix can be described via

This research was supported in part by the National Science Foundation under grants CCR-9875805 and CCR-0113385, and the Office of Naval Research under grant N00014-01-1-0825.

[1] A similar result has also been reported independently in [3].

the array steering and response vectors given by

$$\begin{aligned} \boldsymbol{a}_T(\theta_T) &= \frac{1}{\sqrt{P}}\left[1,\ e^{-j2\pi\theta_T},\cdots,e^{-j2\pi(P-1)\theta_T}\right]^T \\ \boldsymbol{a}_R(\theta_R) &= \frac{1}{\sqrt{Q}}\left[1,\ e^{-j2\pi\theta_R},\cdots,e^{-j2\pi(Q-1)\theta_R}\right]^T \end{aligned} \quad (2)$$

where θ is related to the AoA/AoD variable φ (see Fig. 1) as $\theta = d\sin(\varphi)/\lambda$, and λ is the wavelength of propagation. We consider critical $(\lambda/2)$ spacing. The effect of larger spacings is discussed in [1].

The channel matrix $\boldsymbol{H}(t,f)$ can be generally modeled as [2]

$$\boldsymbol{H}(t,f) = \sum_{n=1}^{N} \beta_n \boldsymbol{a}_R(\theta_{R,n})\boldsymbol{a}_T^H(\theta_{T,n}) e^{j2\pi\nu_n t} e^{-j2\pi\tau_n f} \quad (3)$$

which corresponds to signal propagation over N paths with $\{\theta_{T,n} \in [S_{T_-}, S_{T_+}] \subset [-0.5, 0.5)\}$ and $\{\theta_{R,n} \in [S_{R_-}, S_{R_+}] \subset [-0.5, 0.5)\}$ representing the AoDs and AoAs, respectively, $\{\nu_n \in [-\nu_{\max}, \nu_{\max}]\}$ and $\{\tau_n \in [0, \tau_{\max}]\}$ the Doppler shifts and delays, respectively, and $\{\beta_n\}$ the corresponding path gains. $\tau_{\max}$ denotes the delay spread, $\nu_{\max}$ the Doppler spread, and $[S_{T_-}, S_{T_+}]$ and $[S_{R_-}, S_{R_+}]$ represent the angular spreads.

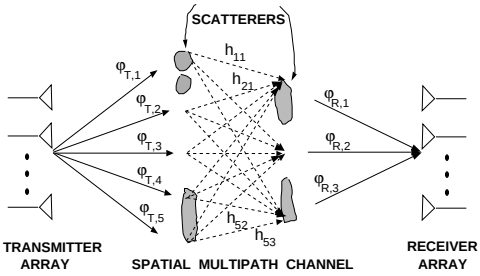

Fig. 1. **Virtual representation** *in the spatial dimension. The virtual angles are fixed a priori and their spacing defines the spatial resolution. The channel is characterized by the virtual coefficients,* $\{H_V(q,p) = h_{q,p}\}$*, that couple the* P *virtual transmit angles,* $\{\varphi_{T,p}\}$*, with the* Q *virtual receive angles,* $\{\varphi_{R,q}\}$*.*

3. VIRTUAL CHANNEL REPRESENTATION

In (3), each propagation path is associated with an AoD, AoA, delay and Doppler shift which can be arbitrarily distributed within the angular, delay and Doppler spreads. As illustrated in Fig. 1, the virtual representation samples the scattering environment at fixed virtual angles, delays and Doppler shifts. The *virtual representation* is expressed as [2]

$$\begin{aligned} \boldsymbol{H}(t,f) &= \sum_{q,p,m,l} H_V(q,p;m,l)\boldsymbol{a}_R(q/Q)\boldsymbol{a}_T^H(p/P) \\ &\quad e^{j2\pi mt/T} e^{-j2\pi lf/W} \end{aligned} \quad (4)$$

corresponding to fixed AoD's, AoA's, delays and Doppler shifts defined as

$$\tilde{\theta}_{T,p} = p/P,\ \ P_- \le p \le P_+,\ \ \tilde{\theta}_{R,q} = q/Q,\ \ Q_- \le q \le Q_+ \quad (5)$$

$$\tilde{\nu}_m = m/T,\ \ -M \le m \le M,\ \ \tilde{\tau}_l = l/W,\ \ 0 \le l \le L, \quad (6)$$

where $L = \lceil W\tau_{\max} \rceil$ denotes the normalized delay spread, and $M = \lceil T\nu_{\max} \rceil$ denotes the normalized Doppler spread. $P_- = \lfloor S_{T_-} P \rfloor$, $P_+ = \lceil S_{T_+} P \rceil$, $Q_- = \lfloor S_{R_-} Q \rfloor$, and $Q_+ = \lceil S_{R_+} Q \rceil$ define normalized angular spreads. The virtual channel coefficients $\{H_V(q,p;m,l)\}$ characterize the linear virtual representation. The spacing between the virtual angles represents the spatial resolutions: $\Delta\theta_T = 1/P$ and $\Delta\theta_R = 1/Q$. The spacing between the virtual Doppler shifts and delays is determined by the spectral and temporal resolutions: $\Delta\nu = 1/T$ and $\Delta\tau = 1/W$.

The virtual coefficients can be computed as

$$\begin{aligned} H_V(q,p;m,l) &= \frac{1}{TW}\int_0^T\int_{-W/2}^{W/2} \boldsymbol{a}_R^H(q/Q)\boldsymbol{H}(t,f)\boldsymbol{a}_T(p/P) \\ &\quad e^{-j2\pi mt/T} e^{j2\pi lf/W} dt df \end{aligned} \quad (7)$$

and they are related to the discrete physical model (3) as

$$\begin{aligned} H_V(q,p;m,l) &= \sum_n \beta_n f_Q(\theta_{R,n} - q/Q) f_P^*(\theta_{T,n} - p/P) \\ &\quad \mathrm{sinc}(m - \nu_n T)\mathrm{sinc}(l - \tau_n W) \end{aligned} \quad (8)$$

were $\mathrm{sinc}(x) = \sin(\pi x)/(\pi x)$ and

$$f_Q(\theta) = \frac{1}{Q}\sum_{i=0}^{Q-1} e^{-j2\pi\theta i} = \frac{1}{Q} e^{-j2\pi\theta\bar{Q}} \frac{\sin(\pi Q\theta)}{\sin(\pi\theta)}. \quad (9)$$

We note that $f_Q(\theta_R)$, $f_P(\theta_T)$, $\mathrm{sinc}(T\nu)$ and $\mathrm{sinc}(W\tau)$ get peaky around the origin with increasing Q, P, T and W.

4. VIRTUAL PATH PARTITIONING

The virtual representation induces a partitioning of propagation paths that reveals the contribution of each path to the DoF, and also exposes fundamental dependencies between the DoF in angle, delay and Doppler. Define the following subsets of paths

$$S_{T,p} = \{n : (p-1/2)/P \le \theta_{T,n} < (p+1/2)/P\} \quad (10)$$
$$S_{R,q} = \{n : (q-1/2)/Q \le \theta_{R,n} < (q+1/2)/Q\} \quad (11)$$
$$S_{\nu,m} = \{n : (m-1/2)/T \le \nu_n < (m+1/2)/T\} \quad (12)$$
$$S_{\tau,l} = \{n : (l-1/2)/W \le \tau_n < (l+1/2)/W\} \quad (13)$$

corresponding to transmit spatial resolution, receive spatial resolution, spectral resolution, and temporal resolution. Note that

$$\begin{aligned} \bigcup_p S_{T,p} &= \bigcup_q S_{R,q} = \bigcup_m S_{\nu,m} = \bigcup_l S_{\tau,l} \\ &= \bigcup_{p,q,m,l} S_{T,p} \cap S_{R,q} \cap S_{\nu,m} \cap S_{\tau,l} = \{1,2,\cdots,N\} \end{aligned} \quad (14)$$

With this path partitioning the virtual coefficients in (4) and (8) can be approximately expressed as

$$H_V(q,p,m,l) \approx \sum_{n \in S_{q,p,m,l}} \beta_n \quad (15)$$

where $S_{q,p,m,l} = S_{T,p} \cap S_{R,q} \cap S_{\nu,m} \cap S_{\tau,l}$. The above equation states that $H_V(q,p;m,l)$ is determined by the sum of gains of all the paths that lie in $S_{q,p;m,l}$, which corresponds to a four-dimensional resolution bin in the neighborhood of the p^{th} virtual

transmit angle, q^{th} virtual receive angle, m^{th} virtual Doppler shift and l^{th} virtual delay.

We assume that each path gain takes the form $\beta_n = \alpha_n e^{j\phi_n}$ where $\{\alpha_n \geq 0\}$ are deterministic path amplitudes and $\{\phi_n\}$ are independent path phases that are uniformly distributed over $[0, 2\pi)$. Thus, we have $\mathrm{E}[\beta_n \beta_{n'}^*] = \alpha_n^2 \delta_{n-n'}$ where δ_n denotes the kronecker delta function. It follows from (15) that the virtual coefficients are approximately uncorrelated since distinct $S_{q,p,m,l}$ correspond to disjoint subsets of paths. The power in each virtual coefficient is given by

$$\sigma^2_{q,p,m,l} = \mathrm{E}[|H_V(q,p;m,l)|^2] \approx \left[\sum_{n \in S_{q,p,m,l}} \alpha_n^2 \right] \qquad (16)$$

which is the sum of powers of all paths in $S_{q,p,m,l}$. Note that even under the assumption of deterministic path amplitudes, each $H_V(q,p;m,l)$ will exhibit Gaussian statistics (Rayleigh fading) for sufficiently large number of paths contributing to it (central limit theorem). On the other hand, as the number of paths contributing to each virtual coefficient decreases, its statistics will deviate from Gaussian towards more "specular" statistics (see next section).

5. DEGREES OF FREEDOM, DEPENDENCIES, AND FADING STATISTICS

The number of dominant non-vanishing virtual coefficients determine the DoF in the channel. The DoF depend on the number of propagation paths, as well the angular and delay spreads associated with them. In a SISO system ($P = Q = 1$), the maximum number of DoF is the number of resolvable delay-Doppler bins: $N_T = (L+1)(M+1)$. In a narrowband MIMO channel, the maximum number of DoF is the number of resolvable spatial bins; $N_S = (P_+ - P_- + 1)(Q_+ - Q_- + 1)$. In a TF-MIMO channel, the maximum number of DoF is

$$N_{ST} = N_S N_T. \qquad (17)$$

The ergodic capacity of a TF-MIMO channel only depends on the angular DoF whereas the DoF in delay-Doppler only contribute to diversity and outage capacity [4].

Equation (17) serves as an upperbound on the spatio-temporal DoF; it assumes that the DoF in angle, delay and Doppler are independent. However, since the DoF are ultimately excited by the same underlying propagation paths, the *effective* spatio-temporal DoF, $N_{ST,eff}$, are in general less than the upper bound N_{ST}. The fundamental dependencies are due to the fact that each virtual angle, delay and Doppler shift corresponds to a subset of paths, as evident from (10)-(13). For illustration, consider a fixed virtual angle pair (q,p). The corresponding $H_V(q,p;m,l)$ are non-vanishing over the (m,l) range defined by

$$L_{-(q,p)} \approx \left[\min_{S_{q,p}} \tau_n \right] W \ , \ L_{+(q,p)} \approx \left[\max_{S_{q,p}} \tau_n \right] W \qquad (18)$$

$$M_{-(q,p)} \approx \left[\min_{S_{q,p}} \nu_n \right] T \ , \ M_{+(q,p)} \approx \left[\max_{S_{q,p}} \nu_n \right] T \qquad (19)$$

Consequently, the virtual representation (4) can be refined to reflect the essential DoF in the channel

$$N_{ST,ess} = \sum_{q,p} \sum_{l=L_{-(q,p)}}^{L_{+(q,p)}} \sum_{m=M_{-(q,p)}}^{M_{+(q,p)}} \leq N_{ST}. \qquad (20)$$

Note that $N_{ST,ess} = N_{ST}$ in (17) if and only if $(L_+ - L_- + 1)(M_+ - M_- + 1) = (L+1)(2M+1)$ for all (q,p); that is, each spatial DoF is associated with maximum DoF in delay-Doppler. This would be true only if there are sufficiently large number of paths ($N > N_S N_T$).

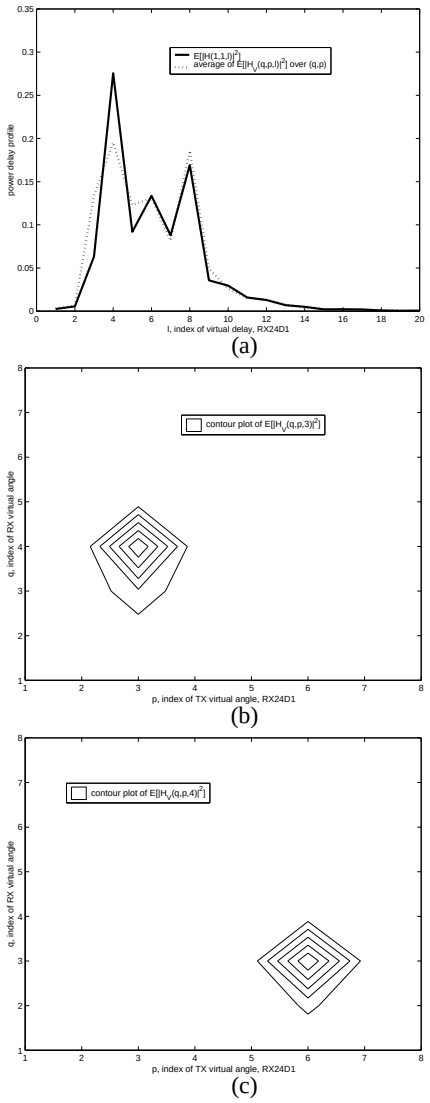

Fig. 2. *Illustration of angle-delay dependencies based on measured data for an 8x8 indoor MIMO channel. (a) Virtual delay power profile. (b) Contour plot of* $\mathrm{E}[|H_V(q,p;3)|^2]$. *(c)* $\mathrm{E}[|H_V(q,p;4)|^2]$.

Conversely, for a given l, the number of non-vanishing entries in the matrix $\{H_V(q,p;l)\}$ (spatial DoF) will be smaller than N_S in general. Specifically, if $N \approx N_S$, then the total spatial DoF (N_S) will be distributed over virtual delays; the spatial matrices $\{H_V(q,p;l)\}$ for distinct delays (l) will be non-vanishing over disjoint sets of entries. These dependencies are illustrated in Fig. 2 which is based on real measured data for an 8x8 wideband ($W =$

120MHz) MIMO system in an indoor environment.[2] Fig. 2(a) shows the virtual delay power profile $\sigma_l^2 = \sum_{q,p} \mathrm{E}[|H_V(q,p;l)|^2]$. Figs. 2(b) and (c) show contour plots of the virtual angle power profile, $\mathrm{E}[|H_V(q,p;l)|^2$, for $l = 3$ and $l = 4$, respectively. Evidently, the path subsets $S_{\tau,l}$ associated with the two adjacent delays exhibit completely disjoint sets of spatial angles, suggesting that $N < PQ = 64$ in this case.

As P, Q, or W increase, the angle-delay DoF $N_{ST} = N_S(L+1)$ increase but the size of the resolution bin associated with each DoF decreases. For fixed N, it follow from (15) that for sufficiently large $N_{ST} > N$, at most a single path will contribute to each bin; that is, $H_V(q,p;l) \approx \beta_{n(q,p,l)}$, where $n(q,p,l)$ is the single path in $S_{q,p,l}$. Consequently, the variation in each non-vanishing virtual coefficient will be entirely due to phase

$$H_V(q,p;l,t) \approx \beta_{n(q,p,l)} e^{j2\pi\nu_{n(q,p,l)}t}. \qquad (21)$$

An immediate consequence of this effect is that even though the marginal statistics of each element of $\boldsymbol{H}(t,f)$ may still be Gaussian, the joint statistics will deviate from Gaussian since the number of paths is smaller than the DoF in the channel. This directly impacts the coherent channel capacity behavior, as illustrated in Fig. 3 for a narrowband MIMO channel. Two channels are simulated in the virtual domain. In one case, the virtual coefficients are modeled as i.i.d. unit variance complex Gaussian (Rayleigh fading), whereas in the other case, the virtual coefficients are modeled with deterministic path amplitudes but independent phases (specular fading). For Rayleigh fading, $\sigma_H^2 = \mathrm{trace}(\boldsymbol{H}_V \boldsymbol{H}_V^H) = PQ$. For specular fading the path amplitudes, $\alpha_{q,p}$, are scaled so that $\sigma_H^2 = \sum_{q,p} \alpha_{q,p}^2 = PQ$. The coherent capacity is given by [5]

$$C = \mathrm{E}[\log_2(\det(\boldsymbol{I} + \rho \boldsymbol{H}_V \boldsymbol{H}_V^H / P))] \ \ (bits/s/Hz) \qquad (22)$$

where $\mathrm{SNR} = \log_{10}(\rho)$, and $P = Q$. The capacity for the two channels[3] is estimated using 500 independent channel realizations. For specular fading, the amplitudes are fixed but the phases are independently chosen over the realizations. As evident from Fig. 3, the two channels exhibit near-identical ergodic capacity but the specular channel exhibits a markedly improved outage capacity performance at SNR = 10dB. We note that the outage capacity of the two channels converges at high SNRs ($>$ 20dB) whereas the advantage of specular channel becomes more pronounced at lower SNRs ($<$ 10dB). Of course, channel estimation becomes more challenging at low SNRs but we believe that this trend towards specular statistics for large signal space dimensions has implications for non-coherent capacity as well.

It is worth noting that the above implications of angle-delay-Doppler dependencies are particularly relevant in ultra-wideband systems due to their extremely high delay resolution (each $S_{\tau,l}$ would likely contain a single path); in fact, evidence of specular statistics in UWB systems has been reported in some recent experimental studies [6]. The association of disjoint spatial DoF with distinct delays (Fig. 2) could be exploited in space-time coding as well as for multiuser signal separation. For example, signals from two different users could be separated via delay-filtering; at appropriately chosen delays, the signals of different users would correspond to non-interfering virtual spatial channels.

[2]We thank Prof. Ernst Bonek of FTW, Vienna for graciously providing the measured data.

[3]The expression in (22) is the true capacity for the Rayleigh channel but strictly speaking a lower bound for the specular channel.

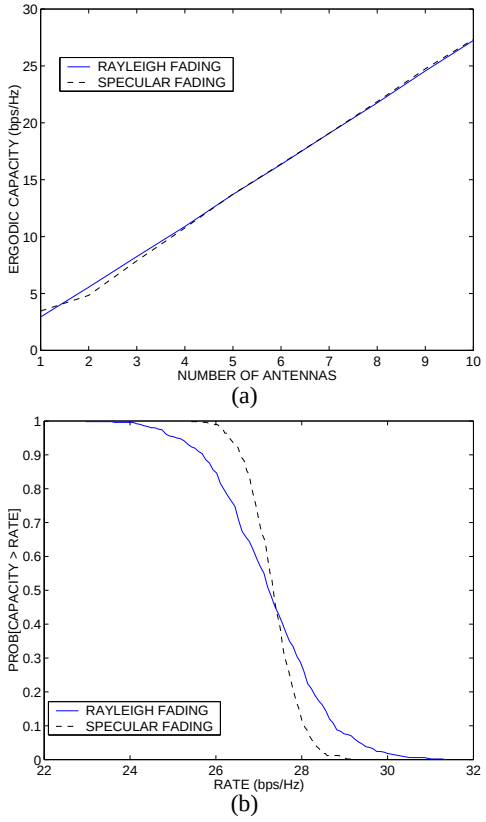

Fig. 3. *Capacity comparison between a Rayleigh fading and specular fading channel at SNR = 10dB. (a) Ergodic capacity. (b) Outage capacity for 10 antennas.*

6. REFERENCES

[1] A. M. Sayeed, "Deconstructing multi-antenna fading channels," *IEEE Trans. Signal Processing*, vol. 50, pp. 2563–2579, Oct. 2002.

[2] A. M. Sayeed and V. Veeravalli, "The essential degrees of freedom in space-time fading channels," in *Proc. PIMRC'02*, (Lisbon, Portugal), pp. 1512–1516, Sep. 2002.

[3] D. Chizhik, "Slowing the time fluctuating MIMO channel by beamforming," *to appear in the IEEE Trans. Wireless Commun.*, 2003.

[4] K. Liu, V. Raghavan, and A. M. Sayeed, "Capacity scaling and spectral efficiency in wideband correlated MIMO channels," *IEEE Trans. Inf. Th.*, pp. 2504–2526, Oct. 2003.

[5] E. Telatar, "Capacity of multi-antenna Gaussian channels," *AT& T-Bell Labs Internal Tech. Memo.*, June 1995.

[6] S. Ghassemzadeh, R. Jana, C. Rice, W. Turin, and V. Tarokh, "Measurement and modeling of an ultra-wide bandwidth indoor channel." Communication Theory Workshop (recent results session), May 2002.